Nuclear Dynamics of Benzene···$(Ar)_n$ Clusters

Jaroslav Vacek and Pavel Hobza*

J. Heyrovský Institute of Physical Chemistry, Academy of Sciences of the Czech Republic, Dolejškova 3, 182 23 Prague 8, Czech Republic

Joshua Jortner

School of Chemistry, Raymond and Beverly Sackler, Faculty of Exact Sciences, Tel Aviv University, Ramat Aviv, Tel Aviv 699978, Israel

Received: June 13, 1997; In Final Form: May 28, 1998

In this paper we report on constant energy molecular dynamics (MD) simulations of nuclear dynamics of benzene−Ar and benzene−Ar_n ($n = 2-7$) clusters, utilizing the ab initio intermolecular potential of benzene−Ar. The dissociation dynamics of benzene−Ar resulting from a nonselective excitation of the intermolecular modes exhibits an excess energy dependence which can be accounted for in terms of the Rice−Ramsperger−Kassel−Marcus (RRKM) statistical theory. The time-resolved isomerization dynamics of benzene−Ar_2 and rigid nonrigid isomerization of benzene−Ar_n ($n = 2-7$) was investigated. The intracluster vibrational energy redistribution (ICVR) in benzene−Ar from an intramolecular vibration to the intermolecular modes is inefficient on the nanosecond time scale for all of the (one quantum or two quanta) vibrational excitation of each mode. The mode selectivity of the ICVR and its linear dependence on the excess vibrational energy were established. The vibrational predissociation (VP) times for single-mode excitations of benzene−Ar are also slow on the nanosecond time scale (>22 ns), in accord with experimental data. The retardation of ICVR and VP of benzene−Ar reflects the bottleneck effect for intracluster vibrational energy flow, due to the considerable frequency mismatch between the high-frequency vibrational modes of benzene ($\omega = 402-2955$ cm^{-1}) and the low-frequency van der Waals vibrational modes ($\omega = 26$ and 40 cm^{-1}).

1. Introduction

The structure, energies, vibrational level structure, electronic−vibrational spectroscopy, and dynamics of molecular clusters[1] are of considerable interest, as these clusters constitute finite systems whose size and number of vibrational degrees of freedom can be gradually changed[2] and which allow for separation of time scales for nuclear motion.[3] A wealth of information has been gathered for M−R_n heteroclusters, which consist of a small molecule (M = HF, Cl_2, I_2)[4−14] or large molecule (M = benzene, anthracene, tetracene, perylene, carbazole)[15−50] bound to a rare gas atom (R = He, Ne, Ar, Kr, Xe). Regarding M−R_n clusters (M = aromatic molecule), with which we shall be concerned in this work, there have been both extensive studies for numerous systems[15−49] and detailed in-depth studies of a few prototypical ones, e.g., the benzene−Ar_n ($n = 1, 2$) clusters.[50−57] High-resolution spectroscopy has rendered precise information on the structure, binding energies, spectral shifts, and intermolecular vibrational nuclear excitations.[50−56] Photoelectron[20,21,31−33,49] and ZEKE[58] spectroscopy provided information on the ionization potentials of M−R_n clusters. These spectroscopic studies were supplemented by theoretical modeling[15] for M−R_n clusters and extensive ab initio calculations[59−62] of the potential energy surfaces of the benzene−Ar cluster. The intramolecular dynamics of M−R_n and of (halogen molecule)−R_n clusters falls into two categories:

(1) Nondissociative Processes. These pertain to intramolecular vibrational energy redistribution (IVR) and to intracluster vibrational energy redistribution (ICVR), which involves vibrational energy flow from the intramolecular vibrational modes to the intermolecular vibrational van der Waals (vdW) modes.[63−67] In addition, cluster isomerization (for small n) between well-characterized isomers[68−74] is expected, and global cluster isomerization (for large n) exhibits rigid−nonrigid cluster "melting".[72−74] IVR and ICVR dynamics has been investigated experimenataly,[63−67] the experimental information on isomerization dynamics is meager, while quite extensive simulation data[22−29,49,68−74] are available.

(2) Dissociative Processes. When the vibrational excitation energy of both the intramolecular modes and the intermolecular vibrational modes exceed the M−R binding energy, vibrational predissociation (VP) of the cluster is energetically favored.

The early studies[5,6] of the VP of the He−I_2 cluster constituted the first clear case of VP in molecular dynamics. Since then, extensive experimental and theoretical studies have been performed[5−14,75−78] on the VP of halogen molecule−rare gas atom clusters. Perhaps the most interesting feature of the VP of these systems is their nonstatistical dynamics.[3,79] The VP lifetimes cannot be accounted for in terms of the statistical Rice−Ramsperger−Kassel−Marcus (RRKM) theory.[80] The intracluster vibrational energy flow from the vibrationally excited halogen molecule to the van der Waals bond is constrained by the considerable frequency mismatch between the molecular and the van der Waals bonds.[3,79] Regarding the nuclear dynamics of M−R_n clusters, experimental studies were conducted on the VP of benzene−Ar,[63] difluorobenzene−Ar,[65] fluorotoluene−Ar,[67] pyrazine−Ar,[81] anthracene−Ar,[64] and tet-

* Address correspondence to this author.

10.1021/jp971943u CCC: $15.00
Published on Web 10/03/1998

racene−R$_n$ (R = Ar, Xe)[66] clusters. For the benzene−Ar cluster in the S_1 ($^1B_{2u}$) electronically excited state, Stephenson and Rice[63] found that the VP lifetimes are surprisingly long, being in the range of 50−100 ns. The VP lifetimes of the *p*-difluorobenzene−Ar in the S_1 state were found by Parmenter et al.[65] to be in the range of 2−200 ns, exhibiting a marked mode selectivity. The VP lifetimes of several vibrations in the S_1 state of aminotetrazine−Ar were found by Levy et al.[81] to be in the range 2.5−16 ns, also exhibiting mode selectivity. Thus the VP dynamics of these large M−Ar clusters is slow, occurring on the 2−200 ns time scale, manifesting the frequency mismatch between the intramolecular modes and the intermolecular vdW modes. In contrast to the long nanosecond VP lifetimes of benzene[63] and of *p*-difluorobenzene−Ar,[65] the VP of *p*-fluorotoluene is much faster, occurring in the time scale of <300 ps,[67] and reflecting the mediating role of the low-frequency internal rotational modes of CH_3 on IVR and VP.[67] For a cluster containing very large molecules, i.e., anthracene−Ar, the VP dynamics in the S_1 ($^1B_{2u}$) electronically excited state is considerably faster than for the corresponding benzene and *p*-difluorobenzene clusters, being in the time domain of 200−500 ps.[64] IVR, ICVR, and VP in M−R$_n$ clusters are intimately related.[63−67,81]

In the bare isolated aromatic molecule only IVR occurs, with the time scales depending on the excess vibrational energy and the density of vibrational states.[79,82] For low frequencies no IVR takes place; for higher frequency modes Fermi resonances may be exhibited, while for high vibrational excitations picosecond IVR lifetimes prevail, e.g., <20 ps for the 1380 cm^{-1} frequency of anthracene.[82] ICVR can occur from low-frequency intramolecular vibrational modes below the IVR onset, in view of the very low vibrational frequencies of the intermolecular vibrational modes. In a M−R cluster where the aromatic molecule M is vibrationally excited by ν_1 quanta (of frequency ω_1), VP can occur parallel to ICVR or sequentially with it. Similarly, IVR may occur prior to ICVR and to VP,[64] and IVR, ICVR, and VP may prevail sequentially. One may also consider back-transfer (BT) from a vdW mode to benzene modes. The general scheme for the dynamics is

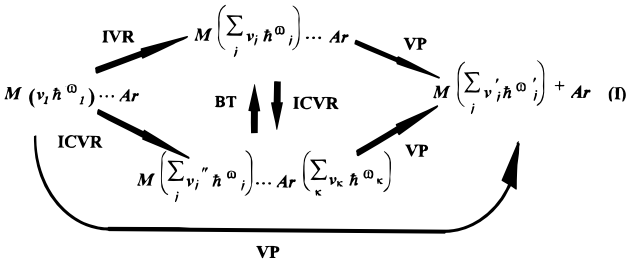

where $\{\nu_j\}$,$\{\nu'_j\}$, and $\{\nu''_j\}$ are the occupation numbers of the intramolecular modes (with frequencies $\{\omega_j\}$) and $\{\nu_\kappa\}$ are the occupation numbers of the intermolecular vdW modes (with frequencies $\{\omega_\kappa\}$).

The direct VP involves coupling to the dissociative continuum. The sequential ICVR−VP process involves the vibrational excitation of the vdW bond (via ICVR) above its dissociation energy ΔE (i.e., $\sum_\kappa \nu_\kappa \hbar\omega_\kappa > \Delta E$) and subsequent dissociation. The sequential ICVR−VP process was proposed on the basis of coupled channel calculations for the VP of the *p*-difluorobenzene−Ar cluster.[33] Several discussions of these mechanisms on the basis of experimental data were provided.[63−67] Intriguing questions remain open concerning the mode selectivity of VP, the role of IVR and ICVR, and the basic mechanisms of VP.

In this paper we address some issues pertaining to the nuclear dynamics of the benzene−Ar and benzene−Ar$_n$ (n = 2−7) clusters. For classical molecular dynamics (MD) simulations of the benzene−Ar cluster ab initio intermolecular potential[59−62] (expressed in terms of superposition of atom−atom potentials) was used. The same potential was utilized for MD simulations of benzene−Ar$_n$, (n = 2−7).[57,60] The benzene intramolecular nuclear motion was described using standard programs.[83,84] The intramolecular force field is anharmonic, with stretching and bending terms being harmonic, and only torsional dihedral terms are anharmonic.[83,84] We focus on the following issues: (1) the exploration of the dissociation dynamics of the benzene−Ar cluster following the nonselective excitation of the vdW modes and the excess vibrational energy dependence of the rate; (2) the isomerization dynamics of (1|1) → (2|0) side crossing between the isomers of benzene−Ar$_2$; (3) rigid−nonrigid isomerization of the benzene−Ar$_n$ (n = 2−7) clusters; (4) intracluster ICVR in benzene−Ar, establishing the time scale, the mode selectivity of these processes, and its dependence on the excess vibrational energy; (5) VP of benzene−Ar under mode-selective excitation of single vibrational modes, establishing the slow (>22 ns) time scale of these processes; (6) the relation between ICVR and VP in the benzene−Ar cluster.

2. Methods

2.1. Intermolecular Potential. The benzene−Ar interaction was described by the ab initio potential[59] which was fitted to the following form of atom−atom interactions:

$$U = \frac{A}{R^\alpha} - B\left(\frac{1}{R^6} - \frac{C}{R^7}\right) \qquad (1)$$

R in eq 1 is the interatomic C−Ar or H−Ar distance, and A−C are the parameters summarized in ref 85a, and α = 13.305. Experimental geometry of the benzene molecule was considered (R_{CC} = 1.406 Å, R_{CH} = 1.08 Å, α = 120°). The ab initio MP2 potential energy surface was generated with the 6-31+G*/7s4p2d basis set.[59,61,62] Formula 1 was also used for the Ar−Ar interaction, and the respective parameters were adjusted to yield the same minimum distance and well depth as that obtained from the 6−12 Lennard-Jones potential;[85b] Ar−Ar parameters are also given in ref 85a. From ref 59 it is evident that this potential reproduces well the ab initio values of the energy and geometry not only for the sandwich structures but also for the planar structures of the benzene−Ar cluster. The largest deviation (about 0.1 kcal/mol) occurred for the C_{6v} structure. We thus expect that the potential (1) will produce the cluster isomer relative energies with accuracy comparable to the ab initio MP2/6-31+G*/7s4p2d treatment. The question now arises about the accuracy of this potential because it is clear that the theoretical level used is not high enough. It was shown previously[86] that passing from MP2 to CCSD(T) level and increasing the AO basis set from 6-31+G*/7s4p2d to 4s3p2d1f/2s1p/6s5p3d2f1g leads to only marginal change of the global minimum stabilization energy (from 351 to 337 cm^{-1}). The close agreement between these two values provides evidence for the reliability of the intermolecular potential evaluated at the MP2/6-31+G*/7s4p2d level. (The actual potential used for MD simulations yields, for the global minimum of benzene−Ar, a stabilization energy of 393 cm^{-1}. This value comes from MP2 calculation with enlarged Ar basis set.) Another argument supporting the quality of this potential comes from refs 51 and 56, where this potential was successfully used for the final assignment of experimental vibrational frequencies of the

benzene−Ar complex. We can conclude by stating that absolute and relative accuracy of the ab initio potential is satisfactory and it is clearly better then the accuracy yielded by any empirical potential. In order to make extensive calculations (of melting and isomerization) more efficient, we used the exponent of $\alpha = 13.0$ in eq 1. The respective parameters $A-C$ were modified to get the same well depth for the benzene−Ar minimum.

The character of stationary points (minimum, saddle point) on the energy surface was unambiguously determined by performing the harmonic vibrational analysis. If all the frequencies are positive, then the stationary point corresponds to a minimum; if some of the frequencies are imaginary, then the stationary point is a saddle point. For benzene−Ar the potential used yields two identical minima (Ar atom is located on the C_6 axes of the benzene, 3.56 Å above and below the ring) and six planar transition states with Ar between two adjacent hydrogens.

2.2. Molecular Dynamics. Two kinds of MD simulations for benzene−Ar_n, ($n = 1-7$) were perfomed, assuming the benzene molecule is rigid (without internal vibrations) and nonrigid.

2.2.1. Rigid Benzene MD. Constant energy MD trajectories were calculated with a fifth-order predictor−corrector integrator[87] in the quaternion space assuming that the benzene molecule is rigid (i.e. free to rotate and translate but without intramolecular vibrations). This method was used for isomerization and melting point calculations. In most cases a 2.5 fs time step was used; it has been shown previously[57] that very similar results were obtained with shorter time steps of 0.5 or 1.0 fs. The MD runs for each cluster were started from the global minimum. Each run consisted of four steps: (i) generation of initial velocities and removing 6 degrees of freedom so that the cluster does not rotate and translate; (ii) equilibration, a short simulation (10^5 steps) with temperature scaling of the velocities; (iii) short time (25 ps) constant energy simulation to test the attainment of required temperature; (iv) constant energy sampling (in order to determine the relative abundances of various isomers of the cluster, rather long sampling (∼100 ns) was carried out). An important characteristic of the cluster under study is the temperature; for rigid benzene simulations the temperature was evaluated as

$$T = \frac{2E_k}{3k_b N_{Ar}} \tag{2}$$

where E_k is the kinetic energy of the cluster, N_{Ar} is the number of argons in the cluster (1−7), and k_b is the Boltzmann constant. From the total number of the degrees of freedom ($3N_{Ar} + 6$) we subtracted six for the overall rotation and translation.

2.2.2. Nonrigid Benzene MD. To model vibrational predissociation of benzene−Ar_n clusters, nonrigid benzene molecule (i.e. free to rotate and translate in space with internal vibrations) constant energy MD simulations are required. AMBER 3.0[83] and AMBER 4.0[84] programs were employed to accomplish the task. A time step of 1 fs was used in most cases to describe the vibrations correctly.

Modified definition of temperature is needed:

$$T = \frac{2E_k}{k_b(3N_{Ar} + 30)} \tag{3}$$

where from the total number of ($3N_{Ar} + 36$) degrees of freedom we subtracted 6 degrees of freedom for the cluster rotation and translation.

2.3. Isomerization Rates Calculations. *First Passage Time Calculations.* The effective isomerization rate can be calculated as reciprocal mean first passage time.[68,69] The mean value of the first passage times $\{t_i\}$ for $i = 1...n$ simulations is

$$\langle\tau\rangle = \frac{1}{n}\sum_{i=1}^{n} t_i \tag{4}$$

and the effective rate constant is $\langle\tau\rangle^{-1}$.

2.4. Melting Temperature Calculations. Rigid−nonrigid transitions of clusters can be investigated using MD simulations.[70−73] The temperature dependence of the internal (total) energy (the caloric curve) of clusters which are characterized by a separated global minimum[74] reveals a step at a temperature which is identified as the cluster melting temperature. Similarly also the standard deviation (of the average Ar−Ar distances changes rather abruptly at the melting temperature.[68,69,72−74]

Short-time constant energy MD simulations with rigid benzene (quaternions) starting from structure equilibrated at different temperatures were performed to study the internal energy−temperature dependence. During the course of MD the average temperature was calculated for each value of total energy together with the standard deviations (of the average Ar−Ar distances. The time step was 2.5 fs; the total length of the simulation was 1.25 ns for each temperature.

2.5. ICVR and Vibrational Predissociation. A classical model of ICVR and vibrational predissociation was considered. The AMBER 3.0[83] potential for benzene was modified first with the aim of reproducing the experimental benzene vibrational frequencies of Goodman et al.[93] The force constants for all dihedral torsions were changed from 5.3 to 15.3 kcal/mol. No improper torsions were used. This leads to an increase in the vibrational frequency of the out-of-plane benzene modes. For example, the lowest vibrational frequency moved from 236 to 402 cm^{-1}. Other features of the potential were found satisfactory. Note that a similar change was introduced in the newer version of the AMBER force field.[84b] Using that potential for the intramolecular part and our ab initio intermolecular potential for the intermolecular part, normal vectors of the benzene−Ar system were calculated. At the beginning of the simulation the cluster was equilibrated with half-quanta excitations in all the intermolecular vdW modes to simulate the zero point energy conditions. After equilibration one selected normal mode of benzene was excited using an algorithm similar to that of Raff.[94] One quantum was used for all modes with a frequency higher than 900 cm^{-1}, and two quanta were used for all modes with a frequency lower than 900 cm^{-1}. During the simulations the Ar "flying average" kinetic energy and "flying average" benzene−Ar distance (average over 5 ps) were calculated and reported.

A time step of 1 fs was used to describe the benzene internal vibrations properly. The simulations were 5 ns long. Ten trajectories were averaged for each normal mode excitation.

3. Dissociation and Isomerization Dynamics

3.1. Benzene−Argon Dissociation. First passage time (FPT) calculations were performed to study benzene−Ar cluster dissociation. At 20 K, 1000 isolated benzene−Ar clusters were equilibrated, followed by a "nonselective" excitation of the van der Waals modes (done by scaling up the velocities). Short-time (100−400 ps) constant energy molecular dynamic runs with rigid benzene were performed. The excitation was designed so that the total energy of the cluster was the same for all the

TABLE 1: Reciprocal Mean First Passage Times $\langle\tau_D\rangle^{-1}$ for Benzene−Ar Dissociation at Different Total Energies δE of the Cluster

δE^a (cm^{-1})	$\langle\tau_D\rangle^{-1}$ (ps^{-1})	δE^a (cm^{-1})	$\langle\tau_D\rangle^{-1}$ (ps^{-1})
100	0.0707	25	0.0243
50	0.0384	10	0.0115

[a] Total energy above the dissociation limit.

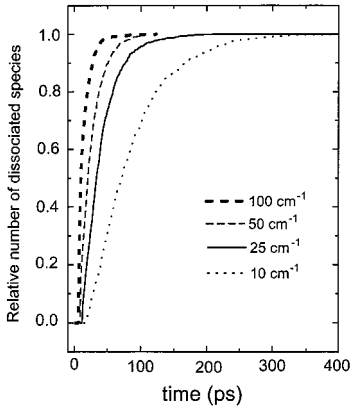

Figure 1. Time dependent number of dissociated species of benzene−Ar for various excess energies above the dissociation limit.

runs. The cluster was considered dissociated if the distance of the argon from the center of mass of the cluster exceeded 7 Å. Calculations were performed for four different values of the total energies (δE) above the dissociation limit (ΔE = 393 cm^{-1}). Results are given in Table 1. $\langle\tau_D\rangle^{-1}$ value is decreasing with decreasing total energy. The time dependence of the number of dissociated species for the excess energies of Table 1 are shown in Figure 1.

Following the simple statistical rate model of Rice−Ramsperger−Kassel (RRK) for dissociation the rate constant $k \equiv \langle\tau_D\rangle^{-1}$ depends on relative excess energy by

$$k = A\left(\frac{\delta E}{\Delta E + \delta E}\right)^{\eta-1} \qquad (5)$$

where A is a frequency factor, $\Delta E = 393$ cm^{-1} is the dissociation energy, δE is the excess internal energy above ΔE, and η is the number of vibrational vdW degrees of freedom. The linear ln(k) dependence on relative excess energy (Figure 2) obeys the RRKM relation. From linear regression we obtained η = 1.85 and $A = 2.1 \times 10^{11}$ s^{-1}. It is well-known that the RRKM theory does not reproduce the experimental results of a unimolecular reaction rate with η being equal to the number of vibrational degrees of freedom [η is usually taken as $\sim\eta_V/2$], as is the case with benzene−Ar dissociation. The low value of the frequency factor is characteristic of the low-frequency vdW motion.

3.2. Benzene−Ar$_2$ Isomerization Rates Calculations. The benzene−Ar$_2$ cluster possesses two minima, a global with (1|1) structure and a local with (2|0) structure (see above and refs 57 and 100), and an isomerization process (called also interconversion) can occur.[70] The benzene−Ar$_2$ isomerization rate $\langle\tau\rangle^{-1}$ was determined using the first passage time calculations done in the same manner as in the case of benzene−Ar dissociation calculation. The simulations were started from the global minimum and continued until the first interconversion to the (2|0) isomer occurred. The time dependencies of the number of interconversions within the specified time are shown in Figure 3 and Table 2.

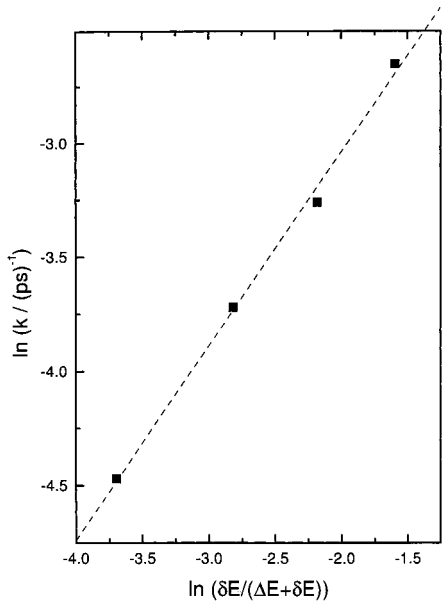

Figure 2. RRK fit (cf. eq 5) for the benzene−Ar dissociation rates.

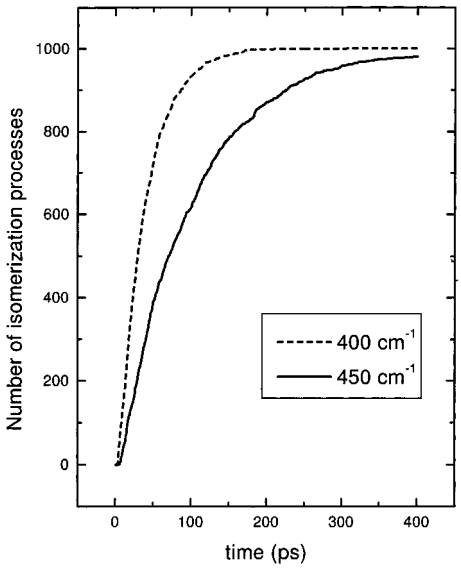

Figure 3. Time dependence of the number of isomerization processes of benzene−Ar$_2$.

TABLE 2: Reciprocal Mean First Passage Times $\langle\tau\rangle^{-1}$ and Rate Constants k_1 and k_2 from Exponential Fits for the Benzene−Ar$_2$ Isomerization Evaluated for Different Total Energies

total energy (cm^{-1})	k_1 (ps^{-1})	k_2 (ps^{-1})	msd[a]	$\langle\tau\rangle^{-1}$ (ps^{-1})
−400	0.015 82	0.009	0.000 6	0.025
−450	0.007 45	0.004 19	0.000 1	0.009 8
−500	0.001 29	0.000 77	0.000 23	0.001 42

[a] Mean square deviation.

3.3. Benzene−Ar$_2$ (1|1) and (2|0) Isomers Time Evolution. The time evolution of the (1|1) and (2|0) isomer populations was also calculated in the energy range from −400 to −500 cm^{-1} (where the zero energy corresponds to the dissociation limit benzene−Ar$_2$ → benzene + Ar + Ar). The ensemble of 1000 trajectories (400 trajectories in the case of the −400 cm^{-1} energy run) was simulated using 1000 different starting conditions at the same total energy. Simulations started from the (1|1) structure and the population of the (2|0) isomer increased until reaching saturation (cf. Figure 4). The calculations were

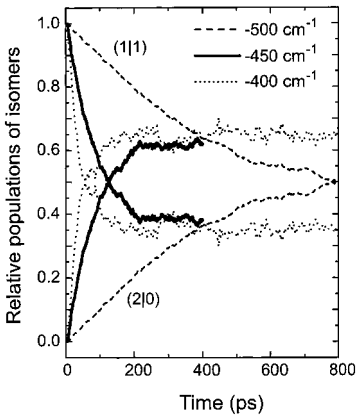

Figure 4. Time dependent isomer populations of benzene−Ar_2 for different total energies.

performed for three different cluster total energies: −400, −450, and −500 cm^{-1}. The equilibrium populations seem to be independent on the total energy (temperature) of the cluster, which is in agreement with previous time averaged data.[57, 100] Even in the case of the total energy of −500 cm^{-1}, the populations are similar to those at higher energies. This simulation is too short to reveal that fact; from the kinetic fit (see next paragraph), we get for the ratio of the equilibrium populations of the two isomers [(1|1)]/[(2|0)] the value of 0.597, which gives the (1|1) equilibrium population of 37.4%. These results are in excellent agreement with previous estimates obtained using time averaging instead of ensemble averaging,[57,100] showing that populations of (2|0) and (1|1) structures were about 63 and 37%, respectively. Higher population of the (2|0) structure was explained by the entropy contribution.

A kinetic modeling of the isomerization was performed for a

$$(1|1) \underset{k_2}{\overset{k_1}{\Leftrightarrow}} (2|0)$$

first-order reactions scheme. The monoexponential decay of the time (t) dependence of the (1|1) population was fitted to obtain the optimal k_1 and k_2 rate constants

$$[(1|1)](t) = \frac{k_2}{k_1 + k_2} + \left(1 - \frac{k_2}{k_1 + k_2}\right) e^{-(k_1+k_2)t} \qquad (6)$$

The time evolutions of the populations as well as the kinetic fits are shown in Figure 4. The evaluated rate constants are summarized in Table 2. There are some differences between $\langle\tau\rangle^{-1}$ and k_1 mainly in the case of the total energy of −400 cm^{-1} when the $\langle\tau\rangle^{-1}$ value is slightly overestimated. Fast "back-hopping" from (2|0) to (1|1), which is not considered in the FPT calculation (mainly important for high-energy simulations), and statistical error are responsible for this difference.

Similarly to in the case of benzene−Ar dissociation, the RRK statistical theory was applied to the benzene−Ar_2 isomerization dynamics (cf. Figure 5). The isomerization barrier $E_B = 220$ cm^{-1} was estimated using quenching simulation. We used

$$k = A\left(\frac{\delta E}{E_B + \delta E}\right)^{\eta-1} = A\left(1 - \frac{E_B}{E_V}\right)^{\eta-1} \qquad (7)$$

where E_V is vibrational excitation and δE is the vibrational excess energy above the isomerization barrier. Using a linear fit of k (cf. Figure 5), we have found $\eta = 4.57$ and a frequency

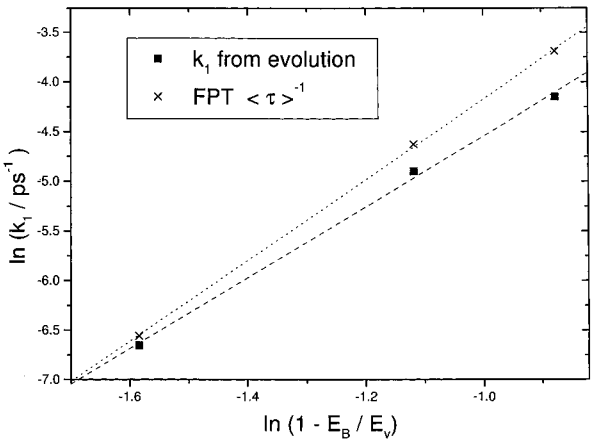

Figure 5. RRK fit (cf. eq 7) for the benzene−Ar_2 isomerization rates.

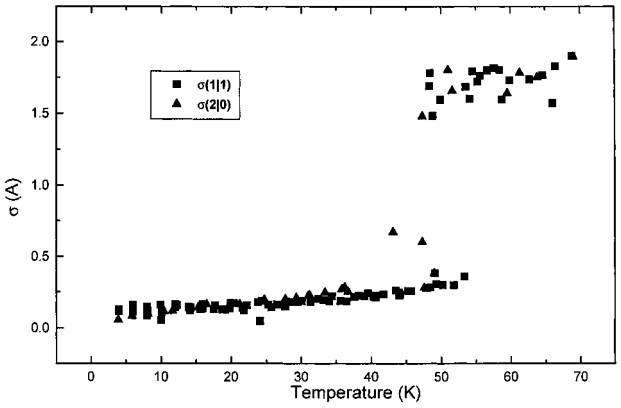

Figure 6. Temperature (T/K) dependence of the standard deviations σ (in units of angstroms) of the average Ar−Ar distances for two-sided (1|1) and one-sided (2|0) isomers of benzene−Ar_2.

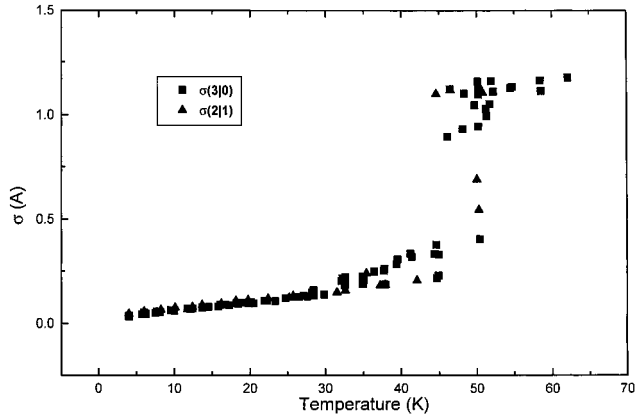

Figure 7. Temperature (T/K) dependence of standard deviations σ (in units of angstroms) of the average Ar−Ar distances for one-sided and two-sided isomers of benzene−Ar_3.

factor $A = 7.6 \times 10^{11}$ s^{-1} for the time evolution simulation and $\eta = 5.07$ and $A = 9.8 \times 10^{11}$ s^{-1} for FPT calculation.

3.4. Cluster Melting. Temperature dependence of the internal energies and the standard deviations σ of the average Ar−Ar distances for different isomers of benzene−Ar_n (n = 2, 3, 7) clusters are shown in Figures 6−9. The melting temperature decreases with an increasing number of argons in the system. For the benzene−Ar_2 the melting point is around 50 K, while it is around 30 K for benzene−Ar_7. At the caloric curve of the benzene−Ar_2 isomers, the (2|0) one is positioned higher in the energy. At the melting temperature the two curves join together. In the case of benzene−Ar_2 the melting temper-

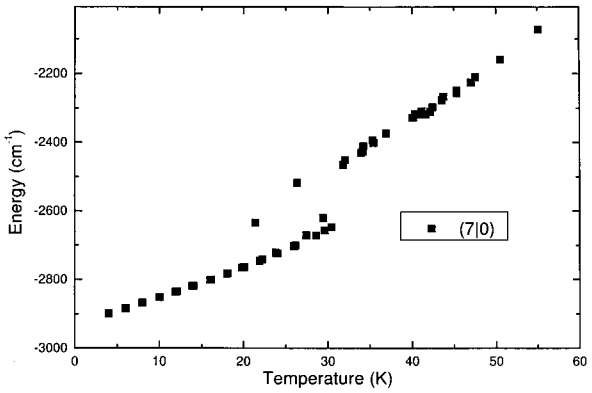

Figure 8. Caloric curve of benzene−Ar_7 isomer. The (7|0) dependence corresponds to the one-sided conformer.

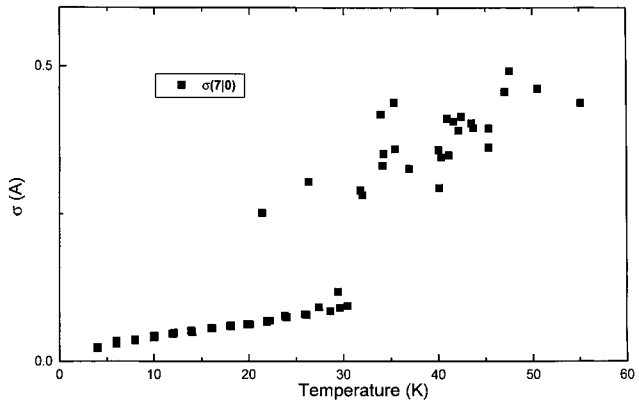

Figure 9. Temperature (*T*/K) dependence of the standard deviations σ (in units of angstroms) of the average Ar−Ar distances for the one-sided isomer of benzene−Ar_7.

ature marks the onset of (1|1) ⇔ (2|0) interconversions. For temperatures below the melting point the probability of side crossing or interconversion is quite low. The frequent side to side crossing above the melting point temperature is responsible for the σ change.[57,100] In all cases the break in the σ curve is sharp. The caloric curves for $n = 2$, 3, and 5 are smooth and featureless. For the benzene−Ar_7 cluster possessing the (7|0) structure there is a jump on the caloric curve (cf. Figure 8) due to large separation between the (7|0) global minimum and the entropically more stable bridged (3|1|3) minima having one Ar in the benzene plane and three Ar atoms on both sides of benzene.[101]

4. Intracluster Dynamics of Vibrational Predissociation of Benzene−Ar

4.1. Mechanisms of VP. The vibrational predissociation (section 2.5) of the benzene−Ar cluster following mode−specific excitation of a single vibrational mode of the benzene molecule was studied. According to scheme I of section 1 we have to distinguish three routes of VP.

(A) Direct VP. This involves direct coupling between the benzene vibrational modes and the dissociative continuum of the vdW mode. Such a mechanism prevails on the case of VP of diatomic molecule−rare gas vdW molecules.[4,5,75,78]

(B) VP Mediated by IVR. In this mechanism intramolecular IVR in the large molecule precedes direct VP. As in mechanism I resonance coupling between intramolecular modes (now accessible by IVR) to the continuum of the vdW mode results in VP.

(C) VP Mediated by ICVR. Sequential transfer of vibrational energy from the intramolecular modes to the vdW modes is followed by VP. For the sequential ICVR−VP process the VP process can be accomplished provided that the energy of the vdW modes (excited via cluster IVR) exceeds the binding energy $\Delta E = 393$ cm^{-1} of the Ar atom to the benzene molecule; i.e., $\Delta E/E_0 \cong 7$, where $E_0 = 53$ cm^{-1} is the ZPE of the vdW modes. For an Ar atom with the total energy ΔE the kinetic energy is $\bar{E}_k \cong (2/3)(\Delta E/2) \cong (7/3)E_0 \cong 130$ cm^{-1}. (We rather report on Ar atom kinetic energy, noting that the normal mode projection procedure of Raff[94] cannot be used for calculations of this nonrigid system.) Since the benzene−Ar potential is very anharmonic, the VP is expected to occur at lower Ar kinetic energy then $E_k = (2/3)\ \Delta E/2 \sim 130$ cm^{-1}.

The three basic mechanisms of VP can prevail sequentially, in reverse (scheme I) and/or simultaneously in parallel. MD simulations of the VP process of benzene−Ar following a mode-specific vibrational excitation in benzene will incorporate all these channels. It is, however, interesting to investigate first the processes of IVR and then turn to the sequential ICVR−VP process.

4.2. IVR in the Benzene Molecule. Intramolecular IVR in the isolated benzene molecule was investigated using the anharmonic force field[83] with the harmonic stretching and bending terms and anharmonic torsional dihedral terms. IVR in benzene was simulated following the vibrational excitation of each of the benzene vibrational modes. This force field is admittedly oversimplified, not containing diagonal and off-diagonal in-plane cubic and quartic terms. The diagonal terms will only modify the vibrational frequencies; however, the in-plane anharmonic nondiagonal terms will affect the IVR dynamics. Thus, our results for the efficiency of IVR dynamics using our anharmonic force field constitute lower limits for the intramolecular dynamics. IVR in benzene induced by high (10 000 cm^{-1}) vibrational excitations was studied by Guan and Thompson.[102] In contrast to the work of Guan and Thompson,[102] we are interested in IVR dynamics at low (single mode) vibrational excitations. All nondegenerate modes and one mode for each degenerate vibration were studied. The excess energy was one vibrational quantum for each mode with energy above 900 cm^{-1} and two vibrational quanta for each mode with energy below 900 cm^{-1}. IVR was specified by the population *P(t)* of the initially excited mode. The characteristic time τ_{IVR} for IVR was characterized by $P(\tau_{IVR}) = 1/e$ and is presented in Table 3. In Table 3 we also present the modes populated during the IVR process, which involve the initially excited mode and other modes effectively coupled to it. These results reveal a marked mode selectivity of the IVR. The IVR dynamics falls into the following categories:

(i) "Inactive" modes exhibiting no IVR on the 10 ns time scale. These involve the 1059 (B_{1u}), 1332 (A_{2g}), 1727 (B_{2u}), and 2955 (B_{1u}) modes.

(ii) Modes characterized by slow IVR, with τ_{IVR} on the nanosecond time scale as well as $\tau_{IVR} > 5$ ns. The initially excited mode in this class is coupled to a small number of modes (Table 3). The majority of the benzene modes fall in this category (Table 3).

(iii) Modes characterized by medium- or high-speed IVR coupled with only a few modes. Sometimes the number of strongly coupled modes is less than three. Then, of course, average excitation energy in the originally excited mode never decreases below *E/e*, *E* being the initial excitation. This is the case of strongly coupled modes 633 (E_{2g}) and 659 (B_{2g}) (cf. Figure 10a−c). Class iii coupling usually occurs for modes with energies close to each other (within 10%). In some cases, however, we can also see overtone coupling, as in the case of

TABLE 3: IVR Dynamics in Benzene for the Mode-Selective Excitation of Different Vibrational Modes, Calculated Benzene Harmonic Frequencies, $\tau_{IVR}(1/e)$ Data, and Specification of the Modes Involved in IVR (See Also Figure 10a−c)

vibrational mode (cm^{-1}) and symmetry	mode no.	$\tau_{IVR}(1/e)$[a]	modes involved in IVR[b]
402/E_{2u}[c]	20	>5000	20
633/E_{2g}[c]	10	>5000	10, 5
659/B_{2g}[c]	5	2300	5, 10, 11
665/A_{2u}[c]	11	>5000	5, 10, 11
880/E_{1g}[c]	6	35	many
917/A_{1g}	2	1870	many
976/E_{1u}	18	>5000	18
1059/B_{1u}	13		13 (no IVR)
1106/E_{2g}	9	>5000	9
1114/E_{2u}	19	>5000	13, 9, 19, 15, 5
1141/B_{2u}	15	450	13, 9, 19, 15, 5
1177/B_{2g}	4	2000	18, 13, 9, 19, 15, 5
1332/A_{2g}	3		3 (no IVR)
1496/E_{1u}	17	>5000	17, 1, 7
1720/E_{2g}	8	>5000	8
1727/B_{2u}	14		14 (no IVR)
2949/E_{1u}	16	>5000	16
2950/A_{1g}	1	15	many
2953/E_{2g}	7	20	many
2955/E_{1u}	12		12 (no IVR)

[a] Characteristic time for IVR in picoseconds. [b] Modes (labeled by their numbers) which are excited after 5 ns. [c] Initial excitation of two quanta was used for all modes with frequency below 900 cm^{-1}; one quantum was used for higher frequency modes. No intramolecular ZPE excitation was applied.

mode 17 (1496 cm^{-1}, E_{1u}) being coupled to modes 1 and 7, having energy close to a 17^2 overtone. Note, that there is no coupling to mode 12 (2955 cm^{-1}, B_{1u}), although it has almost the same vibrational frequency. Overtone coupling is seen also in the case of mode 880 cm^{-1} (E_{1g}), cf. Figure 10. This mode belongs, however, also to class iv (see later) being coupled to a high number of modes. Modes of class iii form groups, and members of such a group are coupled to all other members.

(iv) Modes characterized by fast IVR. These initially excited modes are coupled to a large number of modes (Table 3). These involve the 880 (E_{1g}), 1141 (B_{2u}), 2950 (A_{1g}), and 2953 (E_{2g}) modes.

On the basis of general arguments of intermolecular dynamics in a bound level structure, we expect that the initially excited modes characterized by fast IVR (class iv) correspond to strong coupling with the modes involved in the IVR. In spite of the intrinsic limitations of these conclusions, which depend on the details of the force field used by us for benzene, the conclusion regarding mode specificity of IVR is general. It will be interesting to explore the interrelationship between IVR with the (nonreactive) ICVR and with the (reactive) VP.

4.3. ICVR in Benzene−Ar. We have simulated the ICVR following vibrational excitation of each of the benzene vibrational modes. All the nondegenerate modes and one mode for each degenerate vibration were studied. The excess energy was one vibrational quantum for each mode with energy above 900 cm^{-1} and two vibrational quanta for each mode below 900 cm^{-1}. ICVR to the vdW modes was specified by the time dependence of $E_k(t)/E^0_k$, i.e., the Ar atom kinetic energy $E_k(t)$ at time t relative to its initial ZPE value E^0_k (cf. Table 4). A rough estimate of the characteristic initial time of ICVR was provided by τ_{ICVR} (1.25) for the (initial) increase of the Ar kinetic energy by a numerical factor of 1.25 above its initial value (cf. Table 4). From results presented in Table 4 it can be concluded that intracluster ICVR in benzene−Ar is extremely inefficient on the nanosecond time scale for all of the benzene mode-specific (one-quantum or two-quanta) vibrational excitations. During 5 ns long runs the changes in the kinetic energy of the vdW modes following excitation of the majority of the benzene modes are small; i.e., $E_k(t = 5\text{ns})/E^0_k < 1.2$. In several cases $E_k(t)/E^0_k$ slightly decreases after 200 ps, reflecting minor effects of back-transfer of vibrational energy from the vdW mode to the ring modes. In some cases (e.g., the E_{2g} 2953 cm^{-1} mode) the Ar kinetic energy even decreases unphysically slightly below the ZPE level. Some of the benzene vibrational modes are more efficient for intracluster ICVR. These are the B_{2g} out-of-plane modes (1177 and 659 cm^{-1}), the B_{2u} in-plane-mode (1141 cm^{-1}), the A_{2u} out-of-plane mode (1729 cm^{-1}), and the A_{1g} in-plane mode (917 cm^{-1}) (see Table 4). Even for these most efficient modes, i.e., the B_{2g} (659 cm^{-1}), B_{2u} (1141 cm^{-1}), and B_{2g} (1177 cm^{-1}) vibrations $E_k(t = 5\text{ns}/E^0_k$ does not exceed 1.4 − 1.5 and the ICVR efficiency is very low.

Further information on ICVR (and possibly VP) was inferred from the time dependence of the average benzene−Ar distances. The time dependent average benzene−Ar distances and the Ar kinetic energies induced by one-quantum excitation (two quanta in the case of the B_{2g} 659 cm^{-1} mode) are presented in Figure 11 for these modes, which have the highest ICVR rate. These distances and kinetic energies usually increase up to saturation. Only in the case of energy transfer from the B_{2g} out-of-plane mode (1177 cm^{-1}) does the benzene−Ar distance continue monotonously for the whole simulation (see Figure 11). The average Ar kinetic energy for this mode increases up to saturation (Figures 11−13).

For the most ICVR efficient B_{2g} vibrational mode (1177 cm^{-1}) we tested also how the ICVR depends on the excess vibrational energy. The results are shown in Figures 12 and 13 for excitations of this mode by 0.5, 1, 2, and 4 quanta. In this case 22 ns simulations were performed. As expected, the energy transfer is increasing linearly (see insert to Figure 13) with increasing excitation energy in the mode. Concurrently, for the B_{2g} (1177 cm^{-1}) mode the time dependent benzene−Ar distance (Figure 12) increases slowly for one-quantum vibrational excitation, while for four-quanta vibrational excitation the distance increases linearly at long times, indicating the possibility of VP. The same simulation was performed for the second B_{2g} (659 cm^{-1}) mode. The transfer from this mode is saturated after 1 ns for both two-quanta and four-quanta excitations (see Figure 14) and does not reveal any indication for dissociation.

Mode selectivity of the slow ICVR is exhibited in the benzene−Ar cluster, i.e., the benzene B_{2g} out-of-plane (1177 cm^{-1} and 659 cm^{-1}) vibrations being most efficient. The rate of ICVR is not related to the magnitude of the vibrational quantum, the energy rich modes being absolutely inefficient in ICVR. We also cannot infer that the low-frequency intramolecular energy modes are not more effective; e.g., the lowest frequency E_{2u} (402 cm^{-1}) benzene vibrational mode is also inefficient.

We were not able to establish a correlation between the efficiency of the (slow) ICVR (Table 4) in benzene−Ar and the efficiency of IVR inside benzene (Table 3). Two out of the three most effective modes for ICVR, which are characterized by the shortest values of τ_{ICVR} (1.25) and by the largest values of $E_k(t = 5\text{ ns})/E^0_k$ correspond to class iii of IVR (for the B_{2g} (659 cm^{-1}) and B_{2g} (1177 cm^{-1}) modes), and only the B_{2u} (1141 cm^{-1}) relatively efficient ICVR mode corresponds to class iv of IVR. In general, the IVR process for the majority of the benzene modes (classes ii and iii), which exhibits (Table 3) nanosecond and sub-nanosecond values of ($_{IVR}(1/e)$, is considerably faster than the ICVR process which is ineffective on the 10 ns time scale (Table 4).

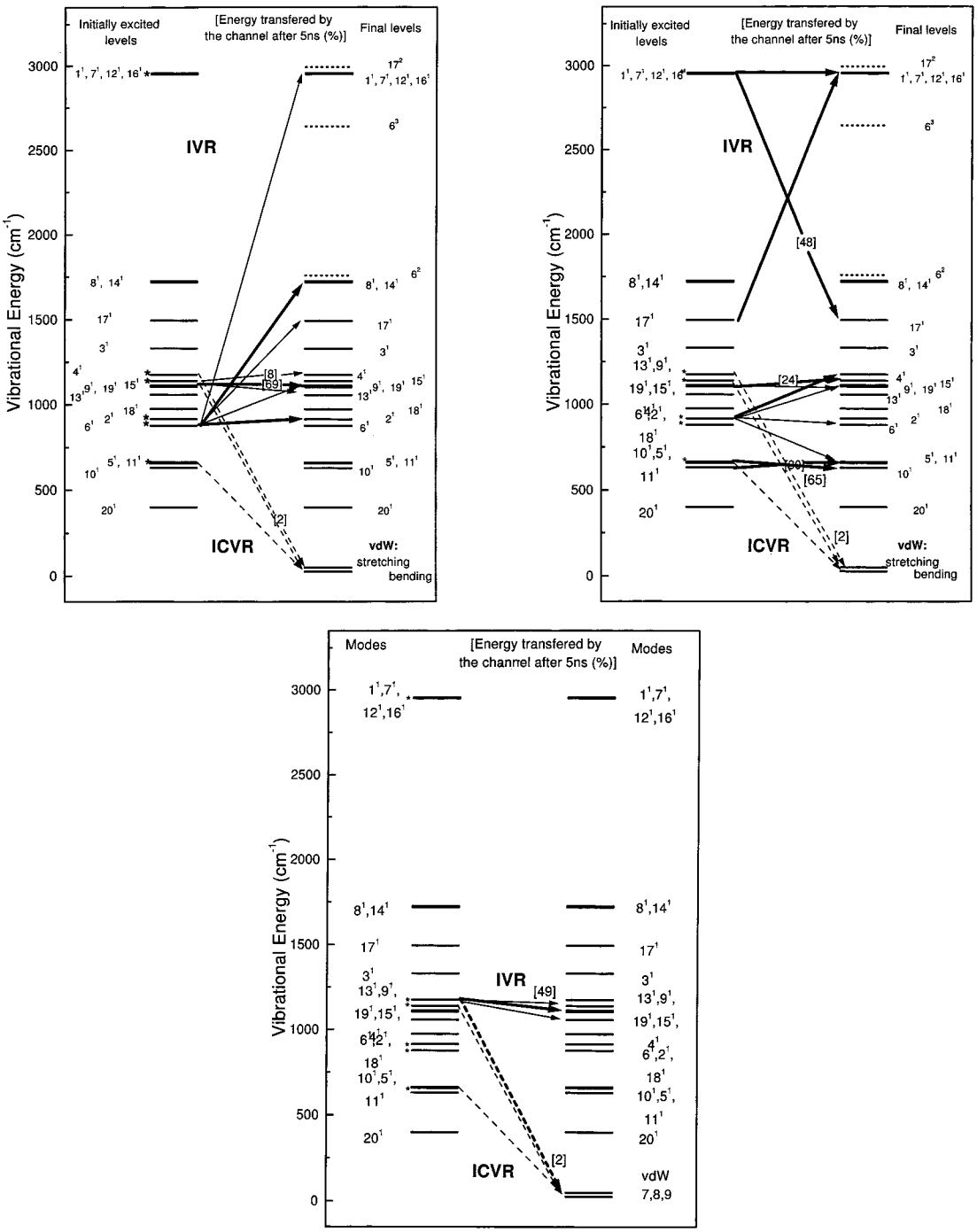

Figure 10. (a (top left), b (top right), c (bottom) Level diagram and IVR efficiency in the benzene−Ar cluster. Levels correspond to vibrational frequencies of the modes. The initial excitation of two quanta was used for all modes with frequency below 900 cm^{-1}; one quantum was used for higher frequency modes. No intramolecular ZPE excitation was applied. Asterisk stand for fast IVR modes. Dotted level lines correspond to overtone levels (in the sense of natural multiples of the fundamental vibrational frequencies). Overtone levels are shown to explain coupling between such modes where one frequency is close to a natural multiple of the other mode frequency (overtone coupling). Numbers in brackets, referring to efficiency of IVR and ICVR channels, show the percentage of energy transferred from the initially excited mode to the final mode after 5 ns.

4.4. VP Dynamics. Our simulations of the VP dynamics of benzene−Ar (Figures 11−14) clearly indicate that for one-quantum excitation for modes above 900 cm^{-1} and two-quanta excitations for modes lower than 900 cm^{-1} the VP is slow on the 10 ns time scale. Three negative results emerge from the search for VP on the 10 ns time scale. Firstly, the low kinetic energies of the Ar atoms (see Figure 13) preclude the direct VP mechanism (A). Our calculations (with the limitations of the intramolecular force field, which was discussed in section 4.2) also indicate that the VP mediated by IVR (mechanism B) is inefficient. Secondly, as for the case of ICVR (section 4.3), there is no correlation between VP and IVR. For the majority of the benzene modes which exhibit nanosecond (classes ii and iii) or sub-nanosecond (class iv) IVR do not induce effective VP on this time scale. Thirdly, the ICVR process is so ineffective that it cannot induce VP on the 10 ns time scale. On the harmonic intermolecular potential surface VP mediated by ICVR (mechanism C) can be realized when $E_k/E^0_k \geq 7$. Our simulations of the B_{2g} (1177 cm^{-1}) mode excited by four quanta on an ab initio anharmonic surface showed, however, that VP can occur as soon as $E_k/E^0_k \geq 3.2$ (see Figure 13 and later in this section). The results simulated with one or two-quanta

TABLE 4: Intracluster ICVR Efficiency in Benzene−Ar for Different Benzene Modes, Calculated Benzene Harmonic Frequencies, the Values of (Initial) $\tau_{ICVR}(1.25)$, and the Kinetic Energy Change $E_k^{(t)}/E^0_k$ (t = 200 ps, 400 ps, and 5 ns)

vibrational mode (cm^{-1}) and symmetry	$\tau_{ICVR}(1.25)^a$	$E_k(200\ ps)/E^0_k{}^b$	$E_k(400ps)/E^0_k{}^b$	$E_k(5ns)/E^0_k{}^b$
$402/E_{2u}{}^c$	>5000	1.00	1.00	0.90
$633/E_{2g}{}^c$	>5000	1.02	1.02	0.75
$659/B_{2g}{}^c$	150	1.30	1.41	1.41
$665/A_{2u}{}^c$	2500	1.06	1.14	1.14
$880/E_{1g}{}^c$	>5000	1.06	1.06	0.90
$917/A_{1g}$	400	1.06	1.25	1.25
$976/E_{1u}$	>5000	1.10	1.18	1.14
$1059/B_{1u}$	>5000	1.06	1.10	0.90
$1106/E_{2g}$	>5000	1.06	1.06	1.00
$1114/E_{2u}$	>5000	0.98	1.00	0.82
$1141/B_{2u}$	200	1.25	1.35	1.45
$1177/B_{2g}$	400	1.14	1.25	1.53
$1332/A_{2g}$	250	1.18	1.14	1.18
$1496/E_{1u}$	>5000	1.06	1.14	1.18
$1720/E_{2g}$	400	1.18	1.25	1.14
$1727/B_{2u}$	180	1.25	1.18	1.06
$2949/E_{1u}$	>5000	1.06	1.14	1.10
$2950/A_{1g}$	>5000	1.06	1.14	0.94
$2953/E_{2g}$	>5000	1.10	1.18	0.86
$2955/B_{1u}$	>5000	1.10	1.14	1.14

[a] In picoseconds. [b] Ar atom kinetic energy change. E_k and $E^0_k = 53\ cm^{-1}$ represent the Ar atom kinetic energy and the Ar atom ZPE, respectively. [c] See footnote c in Table 3.

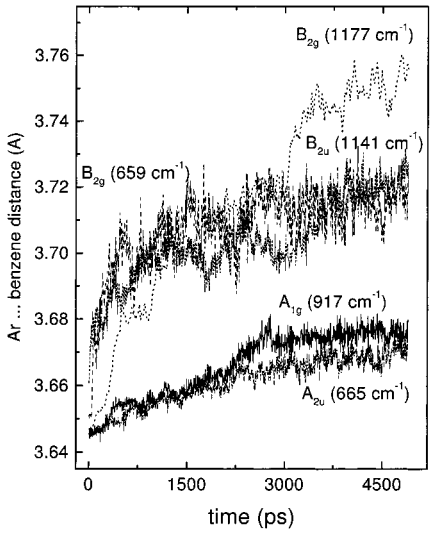

Figure 11. Dependence of the average benzene−Ar distance on time after excitation of the most VP efficient benzene vibrational modes.

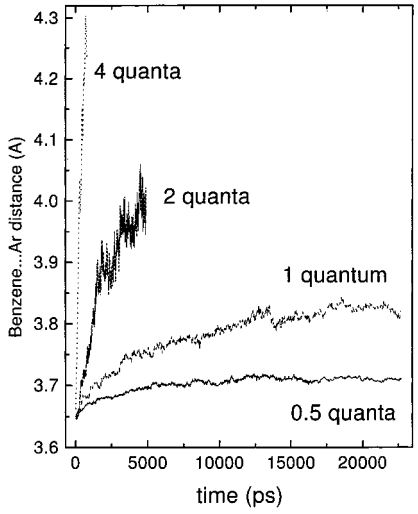

Figure 12. Dependence of the average benzene−Ar distance on time after excitation of benzene vibrational mode B_{2g} ($1177 cm^{-1}$) by 0.5, 1, 2, and 4 quanta.

excitation (Table 4) give for all the modes $E_k/E^0_k \leq 1.5$ (for t = 5 ns), precluding mechanism C on the basis of energy constraints. We thus conclude that, for all the single vibrational excitations of benzene−Ar, all three basic mechanisms (scheme I), i.e., the direct route A, the IVR mediated route B, and the ICVR mediated route C, are slow (>10 ns). Regarding mechanisms A and B, which involve resonant coupling to the energy continuum, we expect these mechanisms to be slow on the basis of the energy gap law for VP.[75−77] What is interesting is the extreme inefficiency of the ICVR mediated VP channel (mechanism C and scheme I), which we shall now further address.

The inefficient intracluster ICVR in the benzene−Ar cluster on the nanosecond time scale following excitation by one vibrational quantum of any of the vibrational modes of benzene precludes the VP route C (induced by one-quantum excitation in the 10 ns time domain). Our simulations showed no VP from any single-mode excitation of benzene−Ar for $t \leq 22$ ns, excluding both sequential and direct VP processes under these vibrational excitation conditions. Only the excitation of very high vibrational states of an ICVR efficient mode can result in a relatively effective VP on the nanosecond time scale. Our only simulations which resulted in VP (on the time scale of ≤22 ns for excess vibrational energy excitation of $<4800\ cm^{-1}$) were those for the most ICVR efficient B_{2g} ($1177\ cm^{-1}$) vibrationally excited mode by four quanta (see Figure 12). From 15 trajectories which were simulated, 13 lead to dissociation. The average dissociation time is 6.8 ± 4.1 ns. Simultaneously with this slow VP process ICVR induced isomerization, e.g., side crossing, occurs in the benzene−Ar cluster. The mean first passage time for side crossing following four-quanta excitation of the B_{2g} ($1177\ cm^{-1}$) mode was 1.03 ± 0.37 ns, reflecting again the slow ICVR in the system.

The major conclusion emerging from our simulations of intracluster ICVR and VP dynamics of the benzene−Ar cluster is that both processes are very slow on the nanosecond time scale. This slow intracluster vibrational energy flow and VP for all of the benzene intramolecular vibrational modes is attributed to a considerable frequency mismatch between the high-frequency vibrational modes of benzene (ω = 402−2955 cm^{-1}, Table 4) and the low-frequency vdW vibrational modes of the benzene−Ar cluster (ω = 26, 40 cm^{-1}, Table 1). The

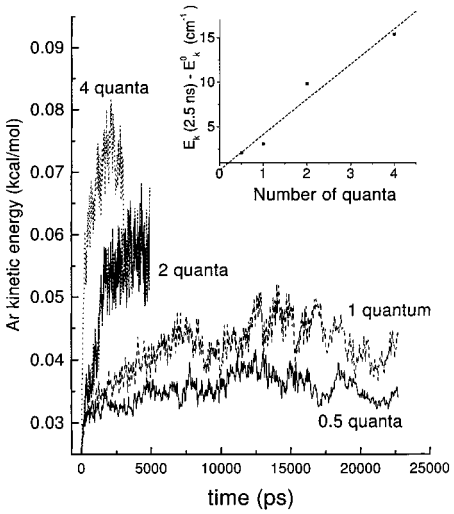

Figure 13. Dependence of the average Ar kinetic energy on time after excitation of benzene vibrational mode B_{2g} (1177cm^{-1}) by 0.5, 1, 2, and 4 quanta. Insert: Vibrational energy transfer from the B_{2g} (1177 cm^{-1}) mode of benzene to the vdW intermolecular modes, expressed by $E_k(t=2.5\text{ns}) - E^0_k$.

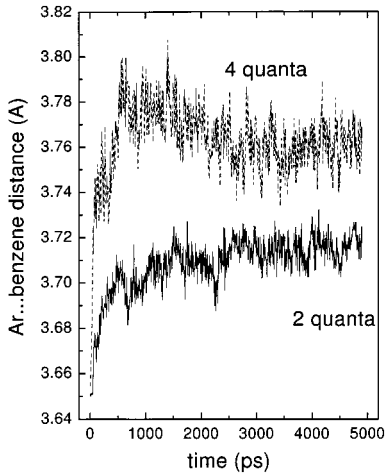

Figure 14. Dependence of the average benzene−Ar distance on time after excitation of benzene vibrational mode B_{2g} (659 cm^{-1}) by 2 and 4 quanta.

bottleneck effect for the intracluster vibrational energy transfer[3,79] makes both intracluster ICVR and consequently also ICVR mediated VP inefficient and slow on the nanosecond time scale.

From our results for ICVR it is apparent that a single-quantum excitation of each of the vibrational modes of benzene−Ar will result in ICVR with $E_t > \Delta E$ and VP only on the long time scale of >20 ns. This conclusion concurs with the results of the experimental study by Stephenson and Rice of the VP dynamics of the $S_1(^1B_{2u})$ electronically−vibrationally excited state of benzene−Ar,[63] where the characteristic VP times for all the optically accessible vibrational states are in the range ≅50−100 ns. This slow VP (and IVR) reflects the bottleneck effect for intracluster vibrational energy flow in benzene−Ar.

How can the VP dynamics of a large (organic molecule)−(rare gas) cluster becomes faster, being pushed into the subnanosecond and picosecond time domain? One has to overcome the bottleneck effect[3,79] for intracluster vibrational energy flow. The vdW vibrational frequencies of (aromatic molecules)−(rare gas) clusters are somewhat lower than those of the benzene−Ar cluster.[15−33] Thus to reduce the dynamics constraints of the bottleneck effect, one has to reduce some of the vibrational frequencies of the aromatic molecule. This will be the situation of the VP of the anthracene−Ar cluster[64] and other clusters of polycyclic aromatic molecules with rare gas atoms[23] in the S_1 state. For the anthracene (S_1)−Ar cluster low intramolecular frequencies will facilitate vibrational energy flow into the vdW modes and VP. Indeed, the experimental results of Zewail et al.[64] for the anthracene (S_1)−Ar cluster reveal VP lifetimes in the range of 200−500 ps. The lowest vibrational frequency of anthracene, which was spectroscopically identified in the S_1 state, is the 209 cm^{-1} B_{3g} out-of-plane vibration.[103] Preliminary simulations of the VP dynamics of the anthracene (S_1)−Ar cluster were performed with the lowest frequency vibrational energy mode being 108 cm^{-1}. This lowest frequency mode corresponds to out-of-plane deformation of the three aromatic rings, resulting in a slow large-amplitude motion of the middle aromatic ring above which the Ar atom is located. The effective coupling between the intramolecular motion and the Ar atom motion is insured. Most important, the low intramolecular frequency allows for good frequency matching between the intramolecular and the VP modes. In our preliminary simulation the 108 cm^{-1} mode was excited by four vibrational quanta, with excess energy exceeding the dissociation limit. The VP time simulated for this excitations is 10 ps, exceeding the corresponding lifetimes for the benzene−Ar cluster by more than 3 orders of magnitude. Of course, there are other significant differences between benzene and anthracene beside the lowest frequency: different mass and momentum ratios in dissociation, higher density of states in anthracene, and hence faster IVR and ICVR and much more anisotropic intermolecular potential. These also contribute to faster VP dynamics of anthracene−Ar clusters. We believe, though, that the 3 order difference in magnitudes of the lifetimes is mainly due to the observed strong coupling between the lowest energy out of plane mode of anthracene and the intermolecular stretching mode. Further studies of intramolecular and intracluster vibrational energy flow in large (aromatic molecule)−(rare gas) clusters will contribute to elucidation of central issues of intramolecular dynamics.

Acknowledgment. This study was partially supported by the Grant Agency of the Czech Republic, Grant No. 203/97/0029.

References and Notes

(1) *Chem. Rev.* **1994**, *94* (7).
(2) Jortner, J. *Z. Phys.* **1992**, *D24*, 247.
(3) Jortner, J.; Levine, R. D. *Isr. J. Chem.* **1990**, *30*, 207.
(4) Houston, J. M. *J. Chem. Phys.* **1992**, *96*, 6752.
(5) Levy, D. H. *Adv. Chem. Phys.* **1981**, *47*, 323.
(6) Beswick, J. A.; Jortner, J. *Adv. Chem. Phys.* **1981**, *47*, 363.
(7) Nesbitt, D. J. *Chem. Rev.* **1988**, *88*, 843.
(8) Ewing, G. E. *J. Phys. Chem.* **1987**, *91*, 4662.
(9) (a) Jucks, K. W.; Miller, R. E. *J. Chem. Phys.* **1987**, *86*, 6637. (b) Dayton, D. C.; Miller, R. E. *Chem. Phys. Lett.* **1988**, *143*, 181. (c) Sato, K.; Achiba, Y.; Nakamura, H.; Kimura, K. *J. Chem. Phys.* **1986**, *85*, 1418. (d) Robinson, R. L.; Ray, D.; Gwo, Dz.-H.; Saykally, R. J. *J. Chem. Phys.* **1986**, *87*, 5149.
(10) Drobits, J. C.; Lester, M. I. *J. Chem. Phys.* **1988**, *88*, 120.
(11) Van der Waals Molecules. *Faraday Discuss. Chem. Soc.* **1982**, 73.
(12) (a) Halberstadt, N.; Beswick, J. A.; Janda, K. C. *J. Chem. Phys.* **1987**, *87*, 3966. (b) Cline, J. I.; Sivakumar, N.; Edvard, D. W.; Janda, K. C. *Phys. Rev.* **1987**, *A36*, 1944. (c) Evard, D. D.; Bieler, C. R.; Cline, J. I.; Sivakumar, N.; Janda, K. C. *J. Chem. Phys.* **1988**, *89*, 2829.
(13) Dixon, D. A.; Herschbach, D. R. *Ber. Bunsen-Ges Phys. Chem.* **1977**, *81*, 145.
(14) Howard, B. J.; Pine, A. S. *Chem. Phys. Lett.* **1985**, *122*, 1.
(15) (a) Even, U.; Amirav, A.; Leutwyler, S.; Ondrechen, M. O.; Berkovitch-Yellin, Z.; Jortner, J. *Faraday Discuss. Chem. Soc.* **1982**, *73*, 153. (b) Leutwyler, S.; Jortner, J. *J. Phys. Chem.* **1987**, *91*, 5558.
(16) (a) Brumbaugh, D. V.; Kenny, L. E.; Levy, D. H. *J. Chem. Phys.* **1983**, *78*, 3415. (b) Alfano, J. C.; Martinez, S. J.; Levy, D. H. *J. Chem.*

Soc., Faraday. Trans. **1990**, *86*, 2503. (c) Heikal, A.; Banares, L.; Semmes, D. H.; Zewail, A. H. *Chem. Phys.* **1990**, *156*, 231.

(17) Leutwyler, S.; Bösiger, J. *Chem. Rev.* **1990**, *90*, 489.

(18) Amirav, A.; Even, U.; Jortner, J. *Chem. Phys. Lett.* **1979**, *67*, 9.

(19) Amirav, A.; Even, U.; Jortner, J. *J. Chem. Phys.* **1981**, *75*, 2489.

(20) Ben-Horin, N.; Even, U.; Jortner, J. *J. Chem. Phys.* **1992**, *97*, 5988.

(21) Ben-Horin, N.; Even, U.; Jortner, J.; Leutwyler, S. *J. Chem. Phys.* **1992**, *97*, 5296.

(22) Jortner, J. *Ber. Bunsen-Ges Phys. Chem.* **1984**, *88*, 188.

(23) Ben-Horin, N.; Bahatt, D.; Even, U.; Jortner, J. *J. Chem. Phys.* **1992**, *97*, 6011.

(24) Leutwyler, S.; Bösiger, J. *Z. Phys. Chem. (Munich)* **1987**, *154*, 31.

(25) Bösiger, J.; Leutwyler, S. *Phys. Rev. Lett.* **1987**, *59*, 1895.

(26) Bösiger, J.; Leutwyler, S. In *Large Finite Systems*; Jortner, J., Pullman, B., Eds.; Reidel: Dordrecht, The Netherlands, **1987**; pp 153−164.

(27) Leutwyler, S.; Bösiger, J. *Faraday Discuss. Chem. Soc.* **1988**, *86*, 225.

(28) Bösiger, J.; Knochenmuss, R.; Leutwyler, S. *Phys. Rev. Lett.* **1989**, *62*, 3058.

(29) Knochenmuss, R.; Leutwyler, S. *J. Chem. Phys.* **1990**, *92*, 4686.

(30) (a) Kelley, D. F.; Bernstein, E. R. *J. Phys. Chem.* **1986**, *90*, 5186. (b) Nimlos, M. R.; Young, M. R.; Bernstein, E. R. *J. Phys. Chem.* **1989**, *91*, 5268.

(31) Schmidt, M.; Mons, M.; Le Calvé, J. *J. Phys. Chem.* **1992**, *96*, 2404.

(32) Schmidt, M.; Mons, M.; Le Calvé, J. *Chem. Phys. Lett.* **1992**, *177*, 371.

(33) (a) Schmidt, M.; Mons, M.; Le Calvé, J.; Millié, P.; Cossart-Magos, C. *Chem. Phys. Lett.* **1991**, *183*, 69. (b) Mons, M.; Le Calvé, J.; Piuzzi, F.; Dimicili, I. *J. Chem. Phys.* **1990**, *92*, 2155.

(34) Hahn, M. Y.; Whetten, R. L. *Phys. Rev. Lett.* **1988**, *61*, 1190.

(35) Bösiger, J.; Bombach, R.; Leutwyler, S. *J. Chem. Phys.* **1991**, *94*, 5098.

(36) Amirav, A.; Jortner, J. *Chem. Phys.* **1984**, *85*, 19.

(37) Amirav, A.; Sonnenschein, M.; Jortner, J. *Chem. Phys.* **1984**, *88*, 199.

(38) Troxler, T.; Leutwyler, S. *Ber. Bunsen-Ges. Phys. Chem.* **1992**, *96*, 1246.

(39) Leutwyler, S. *J. Chem. Phys.* **1984**, *81*, 5480.

(40) Doxtader, M. M.; Mangle, E. A.; Bhattacharya, A. K.; Cohen, S. M.; Topp, M. R. *Chem. Phys.* **1986**, *101*, 413.

(41) Schwartz, S. A.; Topp, M. R. *J. Phys. Chem.* **1984**, *88*, 5673.

(42) Amos, A. T.; Cohen, S. M.; Ketteley, C. J.; Palmer, T. F.; Simons, J. P. In *Structure and Dynamics of Weak Molecular Complexes*; Weber, A., Ed.; Riedel: Dordrecht, The Netherlands, 1987; p 263.

(43) Wittmeyer, S. A.; Kaziska, A. J.; Motyka, A. L.; Topp, M. R. *Chem. Rev. Lett.* **1989**, *54*, 1.

(44) Kaziska, A. J.; Wittmeyer, S. A.; Motyka, A. L.; Topp, M. R. *Chem. Rev. Lett.* **1989**, *154*, 1.

(45) Shchuka, M. I.; Motyka, A. L.; Topp, M. R. *Chem. Phys. Lett.* **1989**, *164*, 87.

(46) Wittmeyer, S. A.; Topp, M. R. *Chem. Rev. Lett.* **1990**, *171*, 29.

(47) (a) Kaziska, A. J.; Wittmeyer, S. A.; Topp, M. R. *J. Phys. Chem.* **1991**, *95*, 3663. (b) Kaziska, A. J.; Shchuka, M. I.; Wittmeyer, S. A.; Topp, M. R. *J. Phys. Chem.* **1991**, *95*, 5017.

(48) Wittmeyer, S. A.; Topp, M. R. *J. Phys. Chem.* **1991**, *95*, 4627.

(49) (a) Bahatt, D.; Heidenreich, A.; Ben-Horin, N.; Even, U.; Jortner, J. *J. Chem. Phys.* **1994**, *100*, 6291. (b) Heidenreich, A.; Bahatt, D.; Ben-Horin, N.; Even, U.; Jortner, J. *J. Chem. Phys.* **1994**, *100*, 6300.

(50) (a) Weber, Th. Thesis, Institut für Physikalische und Theoretische Chemie, Technische Universität München, 1991. (b) Neusser, H. J.; Sussmann, R.; Smith, R. M.; Riedle, E.; Weber, Th. *Ber. Bunsen-Ges. Phys. Chem.* **1992**, *96*, 1252.

(51) Riedle, E.; Sussmann, R.; Weber, Th.; Neusser, H. J. *J. Chem. Phys.* **1996**, *104*, 865.

(52) Sussmann, R.; Neuhausser, R.; Neusser, H. J. *Can. J. Phys.* **1994**, *72*, 1179.

(53) Sussmann, R.; Neuhausser, R.; Neusser, H. J. *Chem. Phys. Lett.* **1994**, *229*, 13.

(54) Sussmann, R.; Neusser, H. J. *J. Chem. Phys.* **1995**, *102*, 3055.

(55) Brupbacher, Th.; Bauder, A. *Chem. Phys. Lett.* **1990**, *173*, 435.

(56) Riedle, E.; van der Avoird, A. *J. Chem. Phys.* **1996**, *104*, 882.

(57) Vacek, J.; Konvička, K.; Hobza, P. *Chem. Phys. Lett.* **1994**, *220*, 85.

(58) Scherzer, W. G.; Selzle, H. L.; Schlag, E. W. *Z. Naturforsch.* **1993**, *48a*, 1256.

(59) Bludský, O.; Špirko, V.; Hrouda, V.; Hobza, P. *Chem. Phys. Lett.* **1992**, *196*, 410.

(60) Vacek, J.; Hobza, P. *J. Phys. Chem.* **1994**, *98*, 11034.

(61) Hobza, P.; Selzle, H. L.; Schlag, E. W. *J. Chem. Phys.* **1991**, *95*, 391.

(62) Hobza, P.; Bludský, O.; Selzle, H. L.; Schlag, E. W. *J. Chem. Phys.* **1992**, *97*, 335.

(63) Stephenson, T.; Rice, S. A. *J. Chem. Phys.* **1984**, *81*, 1083.

(64) Heikal, A.; Banares, L.; Semmes, D. H.; Zewail, A. H. *Chem. Phys.* **1991**, *157*, 231.

(65) (a) Butz, K. W.; Catlett, D. L., Jr.; Ewing, G. E.; Krajnovich, D.; Parmenter, C. S. *J. Phys. Chem.* **1986**, *90*, 3533. (b) Kehn, O. H.; Parmenter, C. S.; Su, M. C. *Ber. Bunsen-Ges Phys. Chem.* **1988**, *92*, 253. (c) Catlett, D. L.; Parmenter, C. S.; Pursell, C. J. *J. Phys. Chem.* **1994**, *98*, 3263.

(66) Penner, A.; Amirav, A. *J. Chem. Phys.* **1993**, *99*, 9616.

(67) (a) Timbers, P. J.; Parmenter, C. S.; Moss, D. B. *J. Chem. Phys.* **1994**, *100*, 1028. (b) Gilbert, B. D.; Parmenter, C. S.; Su, M. C.; Oh, K. H.; Zhao, Z. Q. *Appl. Phys. B*, in press.

(68) Heidenreich, A.; Oref, I.; Jortner, J. *J. Phys. Chem.* **1992**, *96*, 7517.

(69) Heidenreich, A.; Jortner, J. *J. Chem. Phys.* **1992**, *97*, 197.

(70) Ben-Horin, N.; Even, U.; Jortner, J. *Chem. Phys. Lett.* **1992**, *188*, 73.

(71) Jortner, J.; Ben-Horin, N.; Scharf, D. *Theor. Chim. Acta* **1993**, *85*, 199.

(72) Beck, T. L.; Berry, R. S. *J. Chem. Phys.* **1988**, *88*, 3910.

(73) Rose, J. P.; Berry, R. S. *J. Chem. Phys.* **1993**, *98*, 3246.

(74) Bixon, M.; Jortner, J. *J. Chem. Phys.* **1989**, *91*, 1631, 1642.

(75) Beswick, J. A.; Jortner, J. *J. Chem. Phys.* **1978**, *68*, 2277.

(76) Beswick, J. A.; Jortner, J. *J. Chem. Phys.* **1978**, *69*, 512.

(77) Beswick, J. A.; Jortner, J. *J. Chem. Phys.* **1981**, *74*, 6725.

(78) Beswick, J. A.; Delgado-Barrio, G.; Jortner, J. *J. Chem. Phys.* **1979**, *70*, 3895.

(79) Jortner, J.; Levine, R. D. *Adv. Chem. Phys.* **1981**, 47.

(80) (a) Robinson, P. J.; Holbrook, K. A. *Unimolecular reactions*; Wiley: New York, 1972. (b) Forst, W. *Theory of Unimolecular Reaction*; Academic, New York, 1973.

(81) Alfano, J. C.; Martinez, S. J., III; Levy, D. H. In *Mode Selective Chemistry*; Jortner, J., Levine, R. D., Pullman, B., Eds.; Kluwer: Dordrecht, The Netherlands, 1991.

(82) (a) Felker, P. M.; Zewail, A. H. *J. Chem. Phys.* **1985**, *82*, 2961. (b) Felker, P. M.; Lambert, W. R.; Zewail, A. H. *J. Chem. Phys.* **1985**, *82*, 3003.

(83) Singh, U. C.; Weiner, P. K.; Caldwell, J.; Kollman, P. *AMBER 3.0*; University of California: San Francisco, 1986.

(84) (a) Pearlman, D. A.; Case, D.; Caldwell, J.; Singh, U. C.; Weiner, P. K.; Kollman, P. *AMBER 4.0*; University of California: San Francisco, 1992. (b) Cornell, W. D.; Cieplak, P.; Bayly, C. I.; Gould, I. R.; Merz, K.; Ferguson, D.; Spellmeyer, D.; Caldwell, J. C.; Kollman, P. A. *J.Am. Chem.* **1995**, *117*, 5179.

(85) (a) *A*−*C* parameters for Ar−Ar, H−Ar, and C−Ar amount to $0.102\,655\,97 \times 10^8$, 0.145×10^4, 0; $0.220\,76 \times 10^6$, 0.3439×10^3, 2.7149; $0.823\,164 \times 10^7$, 983.5, 0, respectively. A−C are in kcal·$A^{13.305}$/mol, kcal·A^6/mol, and A, respectively (taken from refs 59 and 60). (b) Tang, K. T.; Toennies, J. P. *J. Chem. Phys.* **1984**, *80*, 3726.

(86) Hobza, P.; Selzle, H. L.; Schlag, E. W. *J. Chem. Phys.* **1994**, *94*, 1767.

(87) Heidenreich, A.; Jortner, J. Package of MD programs for molecular clusters, 1992.

(88) Allen, M. P.; Tildesley, D. J. *Computer Simulation of Liquids*; Clarendon Press: Oxford, U.K., 1991.

(89) Gray, S. K.; Rice, S. A.; Noid, D. W. *J. Chem. Phys.* **1986**, *84*, 3745.

(90) Tiller, A. R.; Peet, A. C.; Clary, D. C. *Chem. Phys.* **1989**, *129*, 125.

(91) Garcia-Vela, A.; Villarreal, P.; Delgado-Bario, G. *Int. J. Quantum Chem.* **1989**, *35*, 633.

(92) Waterland, R. L.; Lester, M. I.; Halberstadt, N. *J. Chem. Phys.* **1990**, *92*, 4261.

(93) Goodman, L.; Ozkabak, A. G.; Thakur, S. N. *J. Phys. Chem.* **1991**, *95*, 9044.

(94) Raff, L. M. *J. Chem. Phys.* **1989**, *89*, 5680.

(95) Menapace, J. A.; Bernstein, E. R. *J. Am. Chem. Soc.* **1987**, *91*, 2533.

(96) Schmidt, M.; Mons, M.; Le Calvé, J.; Millié, P.; Cossart-Magos, C. *Chem. Phys. Lett.* **1991**, *183*, 69.

(97) Schmidt, M.; Le Calvé, J.; Mons, M. *J. Chem. Phys.* **1993**, *98*, 6102.

(98) Fried, L. E.; Mukamel, S. *Phys. Rev. Lett.* **1991**, *66*, 2340.

(99) Fried, L. E.; Mukamel, S. *J. Chem. Phys.* **1992**, *96*, 116.

(100) Vacek, J.; Hobza, P. *Int. J. Quantum Chem.* **1996**, *57*, 551.

(101) Vacek, J.; Hobza, P. *J. Phys. Chem.* **1995**, *99*, 17088.

(102) Guan, Y.; Thompson, D. L. *J. Chem. Phys.* **1988**, *88*, 2355.

(103) Lambert, W. R.; Felker, P. M.; Syage, J. A.; Zewail, A. H. *J. Chem. Phys.* **1984**, *81*, 2195.